Blue-Green Systems

IWA PUBLISHING

Comparative study on As(III) and As(V) adsorption by CO_3^{2-}-intercalated Fe/Mn-LDHs from aqueous solution

Yan Tian [ID][a], Guifeng Liu[b], Yingying Gao[b], Yaru Wang [ID][a], Jun Zhang [ID][a], Yali Fang[b], Zongqiang Zhu [IWA] [ID][a] and Huan Deng [ID][a,*]

[a] College of Environmental Science and Engineering, Guilin University of Technology, Guilin 541004, China
[b] Guangxi Key Laboratory of Environmental Pollution Control Theory and Technology, Guilin University of Technology, Guilin 541004, China
*Corresponding author. E-mail: denghuan@glut.edu.cn (H.D)

[ID] YT, 0000-0002-4147-0370; YW, 0000-0002-5443-9276; JZ, 0000-0002-0350-033X; ZZ, 0000-0001-9107-5988; HD, 0000-0002-9400-834X

ABSTRACT

Arsenic pollution prevails in rivers and reservoirs in nonferrous metal mining areas, especially in lead–zinc mining areas, which affects the health of the people residing in such areas. Arsenic usually exists as As(III) and As(V) in water, and the adsorption of As(III) and As(V) changes with the type of adsorbent used. In this work, we report a novel adsorbent Fe/Mn–CO₃-layered double hydroxide (Fe/Mn–CO₃-LDH) composite that can efficiently remove both As(III) and As(V) from water. When the initial concentrations of As(III) and As(V) were 5, 10 and 50 mg/L, the adsorption capacities were 10.12–53.90 and 10.82–48.24 mg/g in the temperature range of 25–45 °C, respectively. The adsorption kinetics conformed well to the pseudo-second-order kinetic model, with all of the fitted correlation coefficients being above 0.998 for all the three initial concentrations (5, 10 and 50 mg/L) tested, suggesting a chemisorption-dominated process. The adsorption isotherms of As(III) and As(V) by Fe/Mn–CO₃-LDHs conformed better to the Freundlich model than to the Langmuir one, indicating a heterogeneous reversible adsorption process. The theoretical maximum adsorption capacity increased with the increase in temperature. During adsorption, As(III) was partially converted to As(V), which was further interacted with intralayer anions. While the electrostatic attraction played an important role in the adsorption of As(V).

Key words: adsorption isotherm, adsorption kinetics, anion intercalation, As(III), As(V), Fe/Mn–CO₃-LDHs

HIGHLIGHTL

- Successful preparation of Fe/Mn–CO₃-LDH material with a high-specific surface area and a large pore volume.
- Pseudo-second-order kinetic model and Freundlich model can all well described the adsorption of As(III) and As(V) on Fe/Mn–CO₃-LDH
- Fe/Mn–CO₃-LDH has good adsorption effect on As(III) and As(V) in a vast range of pH = 2-12.
- pH only have a slight effect on the As(III) adsorbed by Fe/Mn -CO₃-LDH, but obvious for As(V) adsorption.

1. INTRODUCTION

Water pollutants mainly include organic compounds, microbes, heavy metals, etc., among which heavy metals are especially hazardous. Heavy metal elements, which are widely used in industries such as electroplating, chemical manufacturing, oil refinery, leather making, smelting, and mining, enter water bodies predominately through wastewater discharge. Particularly in developing countries, heavy metal wastewater is often discharged unintended into the environment (Deng 2019; Tang et al. 2020). Heavy metals are stable and enduring environmental pollutants due to their poor biodegradability. They can cause irreversible physiological damage upon entering the human body via the food chain. As one of the most toxic heavy metals in the environment, arsenic (As) is toxic for all life forms (Singh et al. 2015). As pollution is very common in rivers and reservoirs in nonferrous metal mining areas, especially in lead–zinc mining areas, which poses a great danger to people's health. Long-term exposure to As can cause lung, liver and kidney cancers and cardiovascular system problems and also affect children's intellectual development (Xu et al. 2010; Sankpal et al. 2012). At present, >70 countries or regions in the world are affected by As pollution, which seriously threatens public health (Zeng et al. 2021). To avoid the direct or indirect impacts of As-containing wastewater on human health and the

environment, the removal of As from water bodies has become a matter of urgent importance. The technologies for As removal mainly include ion exchange, precipitation, membrane separation and adsorption (Choong et al. 2007). Nicomel et al. (2015) found that adsorption was the most effective method, with the advantages of ease of operation and high economic viability. The adsorbent is the core technology of the adsorption method, so the development of excellent adsorbent materials is a prerequisite for realizing large-scale water treatment based on the adsorption technique.

Thc commonly used adsorbent materials for As removal are mainly activated carbon and various metal oxides such as carbon from fly ash (Anna et al. 2006), natural iron ore (Zhang et al. 2004), manganese dioxide (Eleonora et al. 2005) and titanium dioxide (Dutta et al. 2004). Iron compounds have been found to be more effective than other materials for As removal from water (Maiti et al. 2013). The adsorption capacity of iron compounds can be further enhanced by integrating them with manganese oxides to form composite adsorbents, which can have an adsorption capacity of 21.7 mg/g for As (Ociński et al. 2019). The main laminate of Fe–Mn-layered double hydroxides (Fe–Mn-LDHs) consists of a mixed atomic level of bimetallic composite hydroxides, which can make full use of the excellent adsorption properties of iron and manganese compounds. Furthermore, specific anions can be inserted into the interlayers to endow the LDHs with the desired functions. The intercalation modification strategy has been widely applied to prepare advanced LDH-based adsorbents, nano-catalysts, nano-heat stabilizers, mildew preventive, blocking agents and fire retardants (Goh et al. 2008). Ethylenediamine tetraacetic acid-intercalated Mg–Al LDHs were reported to have better adsorption performances for Cu^{2+} and Cd^{2+} (Kameda et al. 2005). Using the one-step solvethermal method, Patel et al. (2017) synthesized the NiCo–LDH nano-foam electrode on a stainless-steel substrate. Sodium dodecyl sulfonate-intercalated hydrotalcite showed strong adsorption properties for reactive brilliant red, acid orange and methyl violet, with the maximum adsorption amounts being 145, 794 and 340 mg/g, respectively (Zhang 2012).

In this paper, a carbonate-intercalated Fe/Mn–CO_3-LDH composite with a layered structure of hydrotalcite was prepared and tested as an adsorbent for As removal from water. The adsorption of As(III) and As(V) by the Fe/MnCO_3-LDH composite was systematically investigated to explore the possible adsorption mechanism. This study provides a new solution to the problem of water resource security in urban ecological planning and construction based on the blue-green system, which can effectively treat As pollution in water bodies and achieve the goal of sustainable use of water resources.

2. MATERIALS AND METHODS

2.1. Preparation of Fe/Mn and Fe/Mn–CO_3-LDHs

Manganese chloride and ferric chloride were chosen as the precursor, and the low saturation co-precipitation method was used to intercalate CO_3^{2-} between the Fe–Mn bimetal hydroxide layers and, thus, synthesize the intercalation of Fe/Mn-LDHs–Fe/Mn–CO_3-LDHs with a layered structure. The detailed preparation process was as follows: 4.505 g of $FeCl_3·6H_2O$ and 6.583 g of $MnCl_2·4H_2O$ were dissolved into 50 mL of ultrapure water to obtain the Fe–Mn-mixed solution, Sol S1. Next, 6.400 g of NaOH and 7.066 g of Na_2CO_3 were dissolved in 100 mL of ultrapure water to obtain the mixed solution, Sol B1. Sol B1 was slowly dropped into 100 mL of ultrapure water in a beaker until pH 12. Then, Sol S1 and Sol B1 were added dropwise to the beaker simultaneously with magnetic stirring. After adding, the mixture was stirred for another 10 min before the beaker was put in a 60 °C water bath kettle for 12 h. After cooling to room temperature, the material was collected through filtration and rinsed three times. Finally, Fe/Mn–CO_3-LDHs were obtained after freeze-drying for 24 h.

2.2. Material characterization

The surface morphology and element composition of the samples were observed and determined using the Japanese field emission JSM-7900F scanning electron microscopy (SEM)-energy-dispersive X-ray spectroscopy (EDS) spectrometer. Material information like crystal structure, lattice parameters and interlayer spacing and the solid-phase structural characteristics were obtained through the X-ray diffraction (XRD) analysis. The functional groups on the sample surface were analyzed using Fourier Transform infrared (FT-IR) spectroscopy. The valence state, chemical bonding and surface element composition of the samples were investigated by X-ray photoelectron spectroscopy (XPS). The pore structure of the material and its specific surface area were measured by using a NOVAe1000 specific surface area and porosity analyzer.

2.3. Static adsorption experiment

Simulated As(III) and As(V) wastewater with concentrations of 5, 10 and 50 mg/L were prepared using $NaAsO_2$ and $Na_3AsO_4 \cdot 12H_2O$, respectively, with 0.01 mol/L NaCl as the background solution. Certain amounts of the Fe/Mn–CO_3-LDH adsorbent and simulated As(III) and As(V) wastewater with various initial concentrations and pH values were taken and placed in a series of polyethylene centrifugal tubes, which were covered and sealed for intensive mixing. The centrifugal tubes were placed in a thermostatic water batch oscillator for the static adsorption experiment at an oscillation rate of 180 r/min until it reached equilibrium.

The initial concentrations of As(III) and As(V) were set as 5, 10 and 50 mg/L, the initial pH values of the solution were adjusted to 2, 3, 4, 5, 6, 7, 8, 9, 10, 11 and 12, respectively, the dose of the adsorbent was set as 0.0300 g/25 mL and the temperature of the thermostatic water bath oscillator was set as 25 °C. Under the same conditions, a blank control experiment was established without the addition of any adsorbent.

When investigating the effect of the adsorbent dose on adsorption, the initial concentrations of the simulated solutions were found to be 5, 10 and 50 mg/L, and the initial pH values of the As(III) and As(V) solutions were adjusted to 7 and 3, respectively. The adsorbent doses were taken as 0.0025, 0.0050, 0.0075, 0.0100, 0.0125, 0.0150, 0.0175, 0.0200, 0.0225, 0.0250, 0.0300 and 0.0375 g/25 mL, respectively, and the experimental temperature was taken as 25 °C.

To investigate the effect of contact time on adsorption, the initial concentrations of the simulated solutions were set as 5, 10 and 50 mg/L. The initial pH values of the As(III) and As(V) solutions were adjusted to 7 and 3, respectively. The adsorbent dose was 0.0125 g/25 mL, the experimental temperature was 25 °C and the samples were taken at 5, 15, 30, 60, 120, 180, 240, 300, 360, 420, 480, 600, 720, 960, 1,220 and 1,440 min, respectively.

To investigate the influences of the initial solution concentration and temperature on As adsorption, the initial concentrations of the simulated liquid were set as 5, 10, 15, 20, 25, 30, 35, 40 and 50 mg/L, respectively. The initial pH values of the As(III) and As(V) solutions were adjusted to 7 and 3, respectively. The adsorbent dose was 0.0125 g/25 mL. The temperatures of the thermostatic water bath oscillator were set as 25, 35 and 45 °C, respectively.

The concentrations of As, Fe and Mn in the solution before and after adsorption were determined using an inductively coupled plasma emission spectrometer (Optima 7000DV).

3. RESULTS AND DISCUSSION

3.1. Material characteristics

3.1.1. Scanning electron microscopy and energy-dispersive X-ray spectroscopy

The morphologies of Fe/Mn–CO_3-LDHs after As adsorption (initial As concentration of 50 mg/L) were observed using an SEM, and the images are shown in Figure 1. It can be seen from the SEM image that after As adsorption, the single crystalline grains of Fe/Mn–CO_3-LDHs still maintained their plate-like morphology and hexagonal crystalline characteristics with distinct edges and corners, and porous structures between lamellas, indicating that the material was relatively stable and its morphologies were not obviously affected by the adsorption.

However, in comparison with the pattern before adsorption (a1 and a2), an apparent agglomeration phenomenon was observed with the LDH layers tiled and piled up after the adsorption of As(V) (c1 and c2). The EDS spectrum (Figure 2) confirmed the presence of an As element on the surface of Fe/Mn–CO_3-LDHs after adsorption and the weight percentage of As was >8.5% (Table 1), suggesting that As was successfully adsorbed onto the material. Compared with the pattern before adsorption, the C and O contents in the material increased to some extent, while the Fe and Mn contents decreased after the adsorption, which might be ascribed to the ion exchange during the adsorption process.

3.1.2. X-ray diffraction

When the saturated solution concentration was 50 mg/L, XRD characterization was performed on the materials before and after adsorption. As shown in Figure 3, the characteristic diffraction peaks (003), (006) and (012) of Fe/Mn–CO_3-LDHs presented favorable multiple relations, indicating the evident layered crystalline structure of this material (Liu 2015; Liu et al. 2020). In comparison with the pattern before adsorption, the intensity of the characteristic diffraction peaks weakened after As adsorption and the (003) peak shifted slightly toward the high-angle position, which were consistent with the structure piling phenomenon shown by the SEM characterization. The two-theta degree of the (003) peak was 11.60° before the adsorption and shifted to 11.78° and 11.73° after the adsorption of As(III) and As(V), respectively. This may be attributed to the change in the charge density
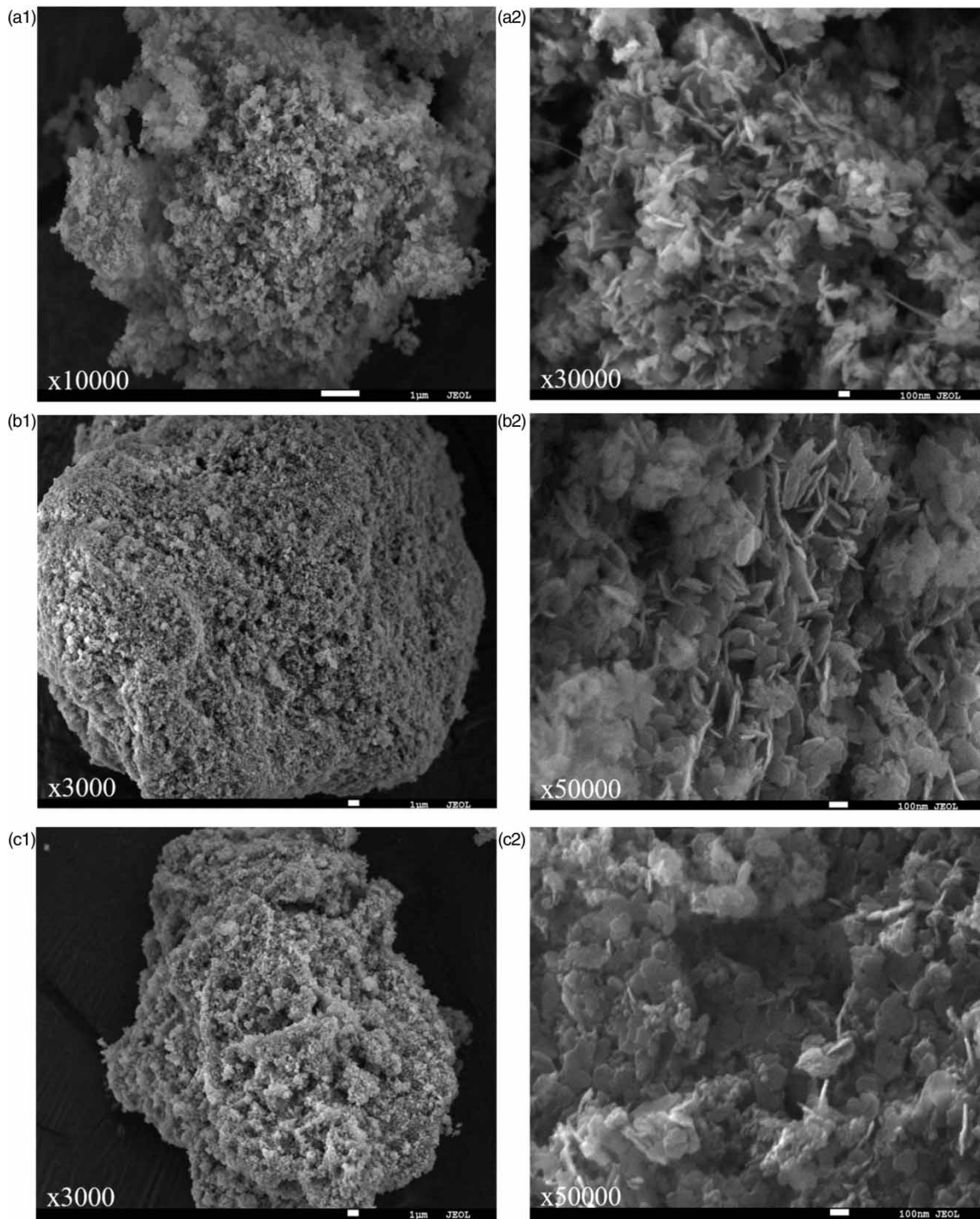
Figure 1 | SEM images of Fe/Mn–CO$_3$-LDHs (a1, a2) before, (b1, b2) after As(III) and (c1, c2) As(V) adsorption.

due to the ion exchange induced by the adsorption of arsenate and arsenite (Halajnia *et al.* 2013; Wan *et al.* 2017). No obvious change was observed for the characteristic peak corresponding to the (110) crystal plane, which might be caused by the collapse of the material structure and pore blocking after the adsorption, which was also consistent with the SEM results.

3.1.3. Fourier Transform infrared

The FT-IR spectra are shown in Figure 4. After adsorption, the strong and broad –OH diffraction peak in the wave number range of 3,200–3,500 cm^{-1} was still present although with a slight shift toward lower frequencies, which
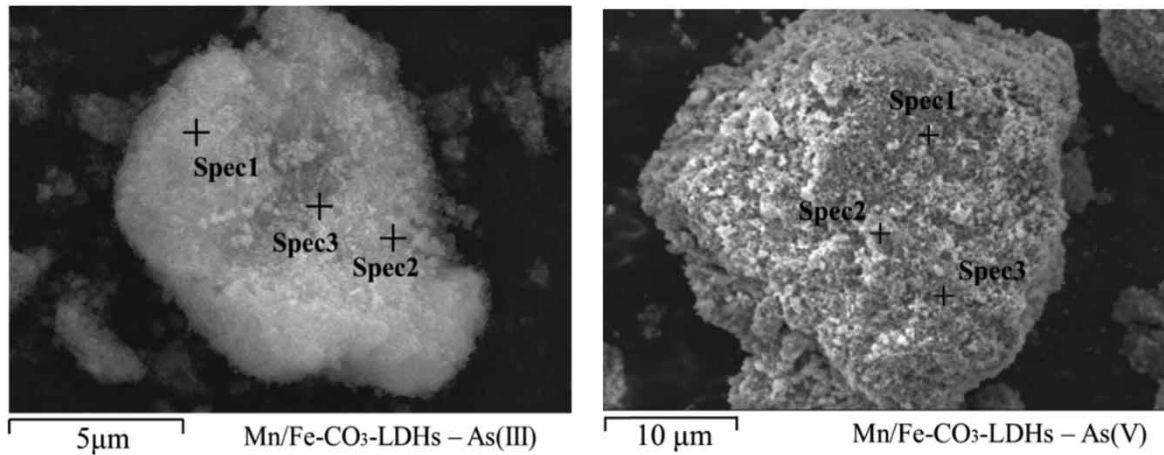
Figure 2 | EDS images of Fe/Mn–CO$_3$-LDHs after adsorption.

Table 1 | Weight percentage of elements in Fe/Mn–CO$_3$-LDHs after adsorption

	Elements	Spectrum 1	Spectrum 2	Spectrum 3	Average
Fe/Mn–CO$_3$-LDHs	C	6.41	5.67	9.11	7.06
	O	27.78	27.14	26.92	27.28
	Mn	44.23	44.80	42.56	43.86
	Fe	21.57	22.40	21.41	21.79
Fe/Mn–CO$_3$-LDHs after As(III) adsorption	C	7.90	9.05	8.55	8.50
	O	28.13	28.71	31.90	29.58
	Mn	36.16	35.02	33.72	34.97
	Fe	19.54	18.72	16.88	18.38
	As	8.26	8.49	8.94	8.56
Fe/Mn–CO$_3$-LDHs after As(V) adsorption	C	7.70	6.57	8.17	7.48
	O	35.55	35.71	37.27	36.18
	Mn	28.88	29.69	26.84	28.47
	Fe	17.45	17.46	16.98	17.30
	As	10.42	10.57	10.74	10.58
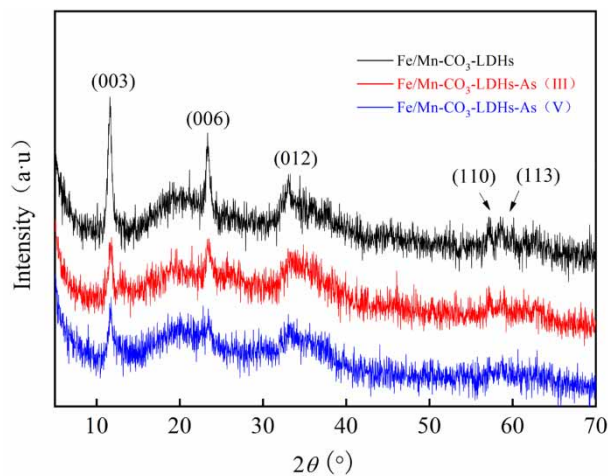
Figure 3 | XRD pattern of the Fe/Mn–CO$_3$-LDHs before and after As adsorption.
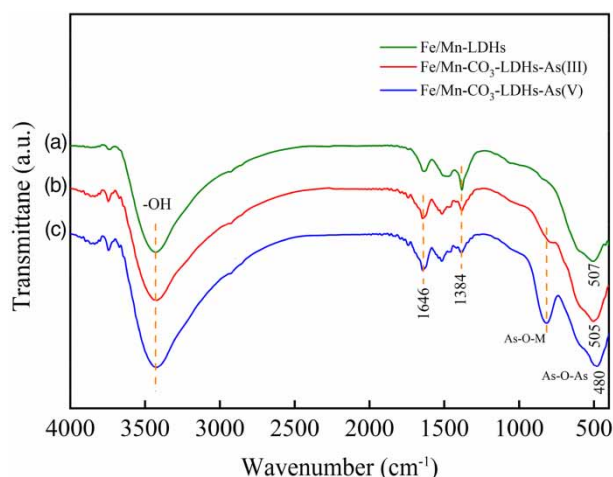
Figure 4 | FT-IR spectra of the Fe/Mn–CO$_3$-LDHs before and after As adsorption.

may be related to the electrostatic interaction between the As anion and the oxygen-containing groups of LDHs (Deng *et al.* 2017). As shown in Figure 4(b) and (c), strong shoulder peaks appeared at 790 and 818 cm^{-1}, which correlated with the formation of Fe–As–O and Mn–As–O bonds. The result indicated that the formation of intra-layer complexes contributed to the As adsorption. The characteristic peak (wave number: 507 cm^{-1}) of the laminate metal lattice in Figure 4(b) shifted to a low frequency after adsorption, confirming that the Fe–O and Mn–O bonds participated in the As adsorption. After adsorption, a new characteristic peak of As–O–As appeared at 505 cm^{-1}.

After adsorption, the vibration peak of CO$_3^{2-}$ (1,384 cm^{-1}) weakened with almost no shift. The highly sym-metrical peak experienced a red shift from 1,492 to 1,460 cm^{-1}, which may be ascribed to the ion exchange of CO$_3^{2-}$ with the As anion during the adsorption process. Because the binding force of CO$_3^{2-}$ to the metal laminate was extremely strong, the presence of the vibration peak of the carbonate (1,384 cm^{-1}) could be attributed to the incomplete ion exchange. The –OH vibration peak of the interlayer water molecules moved from 1,636 to 1,646 cm^{-1}, indicating that the water molecules also participated in the reaction.

3.1.4. X-ray photoelectron spectroscopy

The XPS results of the materials before and after adsorption are shown in Figure 5. The XPS peaks of Fe 2p, Mn 2p, C 1s and O 1s were detected for all samples. A new As 3d peak (44.1–45.6 eV) appeared in the XPS spectra after the adsorption, indicating the successful adsorption of As(III) and As(V) (Wen *et al.* 2014). The high-resolution XPS spectrum of As 3d of the sample after As(III) adsorption could be deconvoluted into two charac-teristic peaks corresponding to As(III) (44.2 eV) and As(V) (45.4 eV), indicating the part oxidation of As(III) to As(V). Only the peak corresponding to As(V) (45.6 eV) existed in the XPS spectrum of the sample after As(V) adsorption, indicating that no As(V) reduction occurred during the adsorption process. It is clear from Figure 5 that there was a significant change in both the intensity and the position of the C 1s peak before and after As adsorption, which might be related to the ion exchange between As and CO$_3^{2-}$ in the adsorption process.

3.2. Analysis of influencing factors on As adsorption

3.2.1. Initial pH of solution

As shown in Figure 6(a), with the initial pH of the solution varying from 2 to 10, the uptake of As(III) remains basically constant, which is credited to the unique adsorption mechanism, i.e. surface complexation between the functional groups on the adsorbent surface and As(III) (Chandra *et al.* 2010; Zhang 2018). When pH < 9, As(III) exists in the nonionic form (H$_3$AsO$_3$) and no electrostatic interaction prevails between the material surface and the adsorbate. As(III) is activated to As(V) by the ligand exchange with hydroxyl groups followed by an inter-action with Fe (Zhu *et al.* 2014). When pH > 9, As(III) mainly exists as H$_2$AsO$_3^-$, HAsO$_3^{2-}$ and AsO$_3^{3-}$, which repels the negatively charged adsorbent surface due to the electrostatic repulsion. However, when pH 9–10, the adsorbent still shows a high adsorption capacity for As(III) (Smedley & Kinniburgh 2002). When pH > 10, the adsorbent experiences a severe hydroxylation process with a significant increase in the negative charge
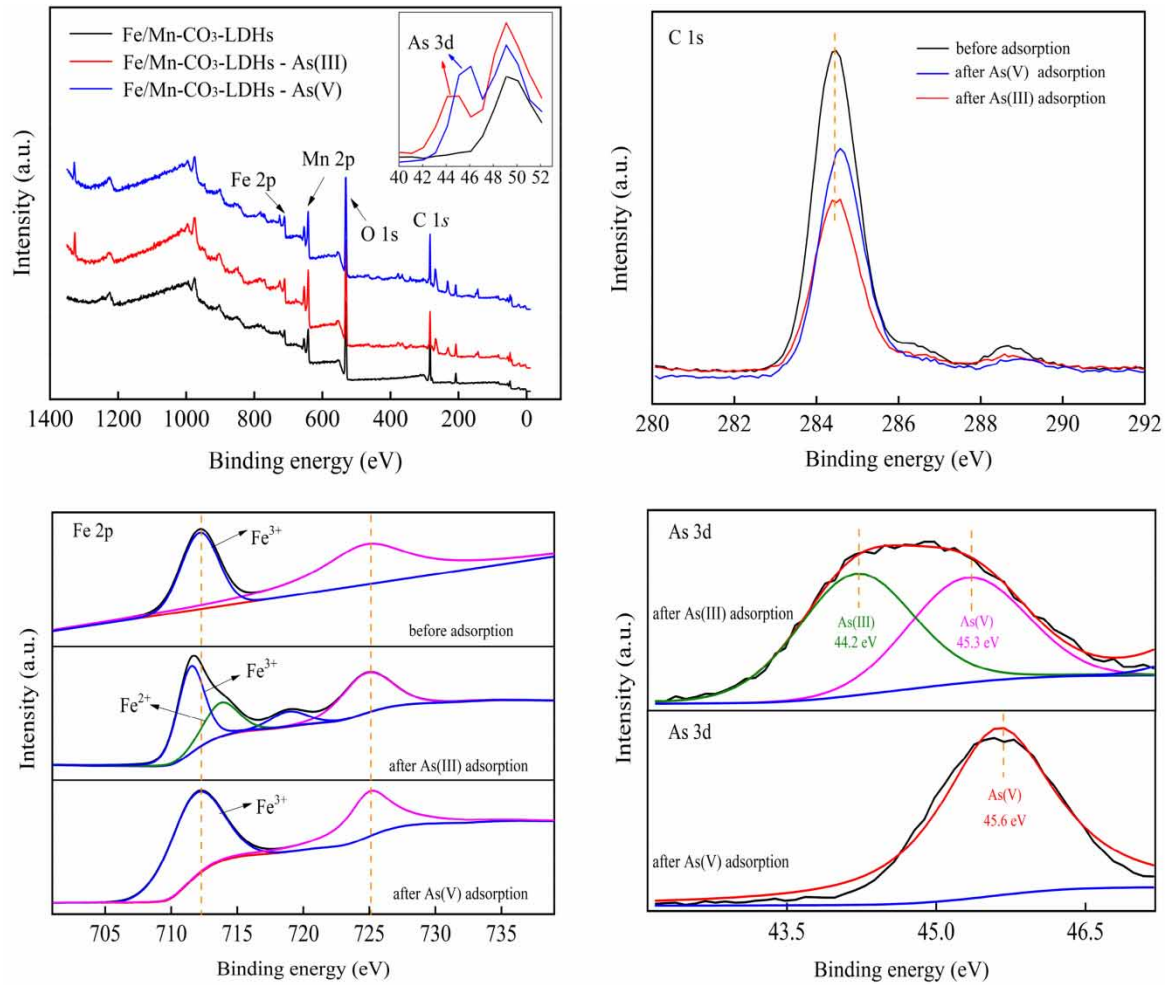
Figure 5 | XPS spectra of the Fe/Mn–CO$_3$-LDHs before and after As adsorption.
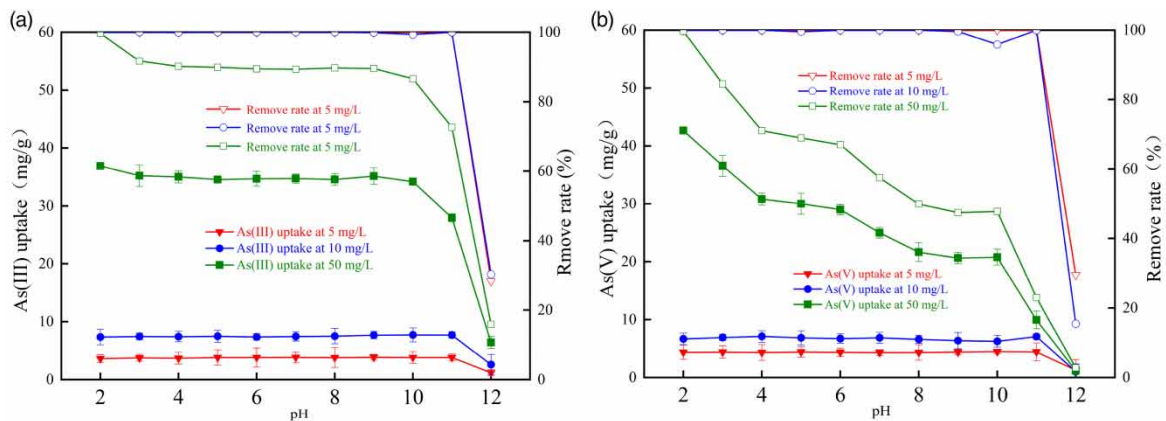
Figure 6 | Effect of initial pH on As(III) and As(V) adsorption (initial concentration 5–50 mg/L; 25 °C).

on the material surface, leading to a reduced adsorption capacity due to an enhanced electrostatic repulsion between the adsorbent's surface and the adsorbate. In accordance with these results, the following As(III) adsorption experiment was performed at an initial pH value of 7.

As shown in Figure 6(b), the optimal initial solution pH for As(V) adsorption by Fe/Mn–CO$_3$-LDH was 2. But the postadsorption pH values of solution were determined to be 3.19 (5 mg/L), 2.98 (10 mg/L) and 2.98 (50 mg/L), respectively. Considering that the solution was still acidic, a dissolution of the LDHs laminate

may have occurred under strong acid conditions (Lv 2005; Li *et al.* 2009). Although the adsorption capacity of As(V) was slightly poor when the initial solution pH increased from 2 to 3, the pH values of the solution post adsorption were approximately neutral, being 6.27 (5 mg/L), 6.82 (10 mg/L) and 6.69 (50 mg/L), respectively. When the solution pH increased from 2 to 12, the adsorbent surface gradually transformed from positive charge to negative charge, with the electrostatic force between the adsorbate and the adsorbent changing from a weak attractive one to a strong repulsive one. Consequently, the As(V) uptake was strongly dependent on the solution pH, with the adsorption capacity waning from 42.66 to 1.19 mg/g. The optimal pH value for the As(V) adsorption by Fe/Mn–CO_3-LDHs was determined to be 3 while considering the adsorption capacity, post-adsorption solution pH and leaching of metal ions from the adsorbent.

3.2.2. Adsorbent dosage

As shown in Figure 7(a), the normalized uptake of As(III) by Fe/Mn–CO_3-LDHs reduced gradually with the dose increase, and the removal rate of As(III) increased gradually and then became stable. When the dose of Fe/Mn–CO_3-LDHs increased from 0.0025 to 0.0375 g/25 mL, the normalized uptake of As(III) with the initial concentrations of 5, 10 and 50 mg/L reduced from 28.88, 34.76 and 60.40 mg/g to 3.34, 6.68 and 31.03 mg/g, respectively. When the dose of Fe/Mn–CO_3-LDHs was 0.0125 g/25 mL, the removal rates for As(III) at the initial concentrations of 5, 10 and 50 mg/L were 99.08, 99.78 and 95.75%, respectively. Taking into account the normalized adsorption capacity, the removal rate and the utilization rate of the adsorbent, 0.0125 g/25 mL was taken as the adsorbent dose in the subsequent experiment.

It can be known from Figure 7(b) that with the change in the dose from 0.0025 to 0.0375 g/25 mL, the normalized uptake of As(V) by Fe/Mn–CO_3-LDHs decreased from 46.75, 57.89 and 57.10 mg/g to 3.75, 7.505 and 34.05 mg/g for the solution at the initial As(V) concentrations of 5, 10 and 50 mL, respectively. Also, the corresponding removal rate increased from 82.58, 51.09 and 10.54% to 99.49, 99.37 and 94.31%, respectively. With the adsorbent dose of 0.0125 g/25 mL, the removal rate of As(V) > 98% was achieved for the solution with both low and medium initial concentrations. The residual As(V) concentrations in the sample were measured as 0.055 and 0.193 mg/L, respectively. Since the available sites normalized to the adsorbent mass were limited, increasing the adsorbent dose was favorable for As(V) removal. However, the removal rate plateaued at a certain dose and an excessive dose was unfavorable for the adsorbent dispersion in the solution. Moreover, excessive dose can also lead to reduced adsorption efficiency. Therefore, the adsorbent dose for the subsequent experiments was 0.0125 g/25 mL.

3.2.3. Contact time

Figure 8 presents the impact of reaction time on As adsorption. As shown in Figure 8(a), the adsorption capacity increased rapidly in the initial adsorption phase, which accounted for 82, 72 and 72% of equilibrium adsorption capacity when the initial As(III) concentrations were 5, 10 and 50 mg/L, respectively. The time required to reach As(III) adsorption equilibrium with the initial concentrations of 5 and 10 mg/L were 360 and 960 min with the respective adsorption capacities of 10.24 and 20.27 mg/g. When the initial As(III) concentration was 50 mg/L,
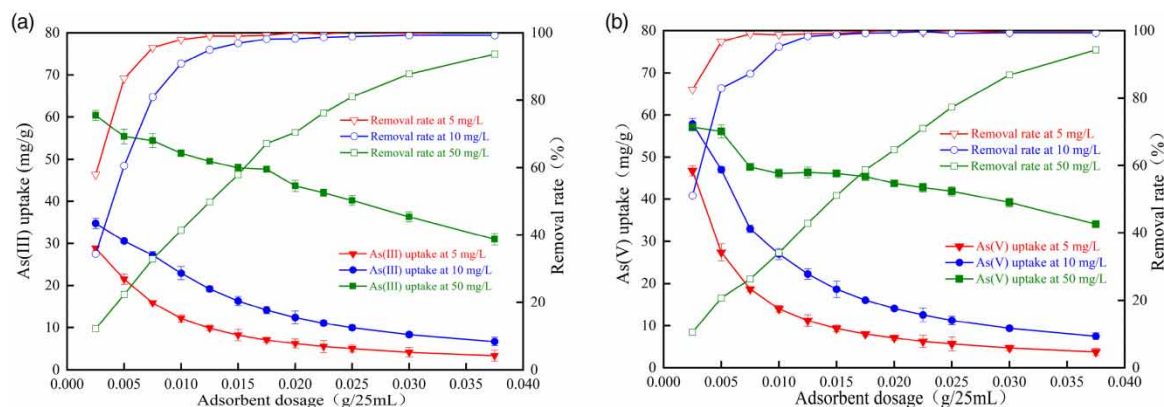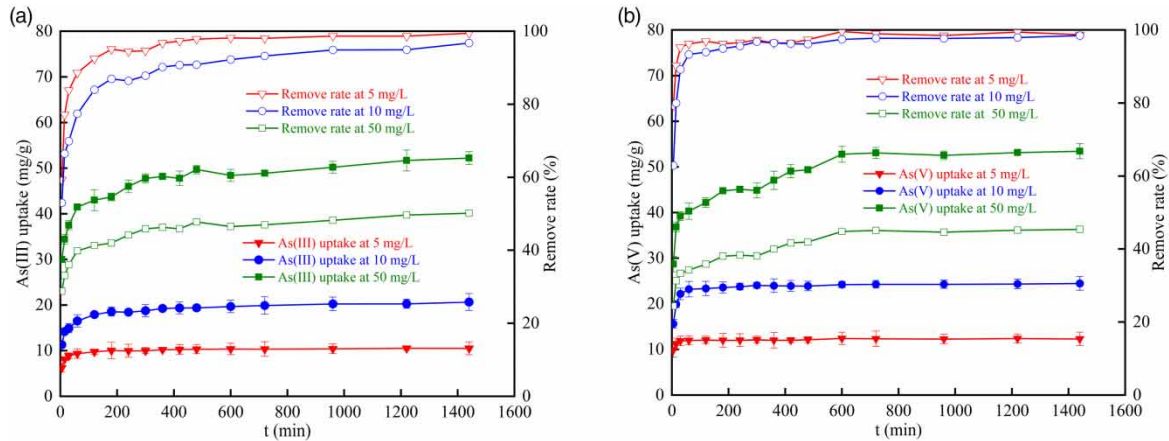

Figure 7 | Effect of Fe/Mn–CO_3-LDHs dose on arsenic adsorption.

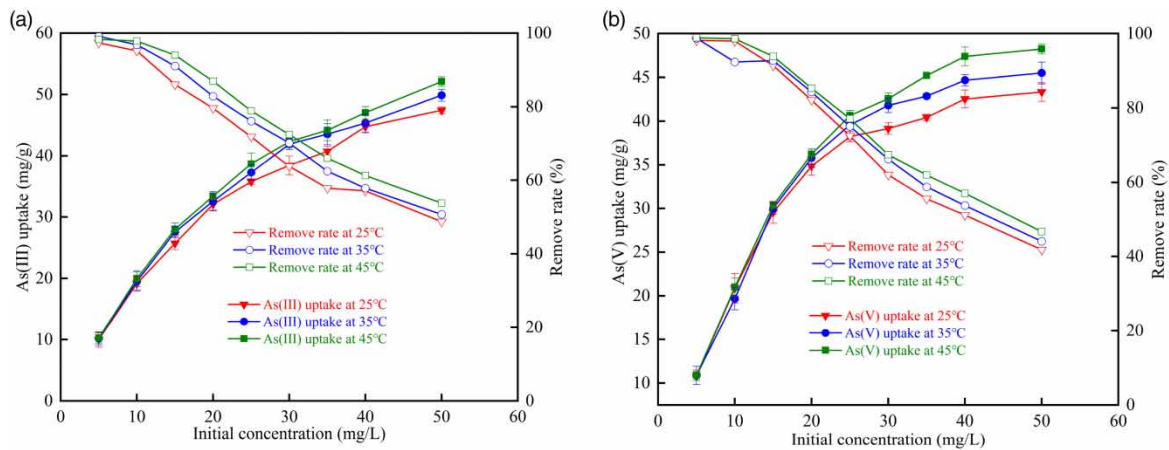**Figure 8** | Effect of time on arsenic adsorption.

the adsorption reached equilibrium within 1,220 min with an adsorption capacity of 51.7 mg/g. The time required to reach equilibrium prolonged with the increase of the initial As(III) concentration.

As shown in Figure 8(b), the time required to reach equilibrium prolonged from 120 to 720 min when the initial As(V) concentration increased from 5 to 50 mg/L. The As(V) uptake fluctuated in a small range when the adsorption gradually approached equilibrium. The time required to attain equilibrium were 120, 600 and 720 min for the initial As(V) concentrations of 5, 10 and 50 mg/mL, respectively, and the corresponding As(V) uptake was 12.09, 24.23 and 50.05 mg/g. The removal rates were higher than 95% for all the tested As(V) concentrations. When the initial As(V) concentration was 5 mg/L, >90% As(V) adsorbed within only 15 min.

3.2.4. Initial concentration and temperature

As shown in Figure 9(a), in the studied concentration and the temperature range, the As(III) uptake increased, while the removal rate reduced with an increase in the initial concentration and temperature. The removal rate increased dramatically with an increase of the initial As(III) concentration up to 25 mg/L, followed by a slow increase with a further increase of the initial concentration. When the initial As(III) concentrations were 5, 10 and 50 mg/L, the As uptake increased from 48.86 to 50.84 and 53.90 mg/g, with the temperature increasing from 25 to 35 °C and finally to 45 °C, respectively. Therefore, temperature increase was favorable for As(III) adsorption.

The influence of the initial solution concentration and temperature on As(V) adsorption is shown in Figure 9(b). Similar to As(III), the As(V) uptake increased with an increase in the adsorbent concentration, while the As(V) removal rate presented an opposite trend. On the one hand, the amount of As(V) anions in the solution phase increased with the increase of the initial concentration. On the other hand, the available adsorption sites that could be provided by a certain amount of adsorbent were limited. As a result, the difference between the

Figure 9 | Effect of initial concentration and temperature on arsenic adsorption.

As(V) concentration in the solid and solution phases aggravated with the increase of the initial As(V) solution, which favored the As(V) adsorption. However, the As(V) concentration at equilibrium also increased, leading to a decrease in the As(V) removal rate according to the Langmuir adsorption model, which will be discussed next.

Temperature played a critical role in the As(V) adsorption when the initial AS(V) concentration was >25 mg/L. A pronounced As(V) uptake increase was observed with the increase in temperature, rising from 43.22 to 45.54 and 48.24 mg/g with the temperature increasing from 25, 35 and 45 °C, respectively, when the initial As(V) concentrations were 5, 10 and 50 mg/L.

From Table 2, it can be clearly seen that Fe/Mn–CO$_3$-LDHs have superior adsorption capability toward As to other materials.

3.3. Adsorption isotherm

The adsorption isotherm is a curve describing the relationship between equilibrium adsorption capacity and solution concentration. The adsorption isotherm data are usually fitted with the Langmuir (Equations (1) and (2)) and Freundlich (Equation (3)) adsorption isothermal models (Qi & Pichler 2016), the formulas of which are as follows:

$$\frac{C_e}{q_e} = \frac{C_e}{q_m} + \frac{1}{q_m K_L} \tag{1}$$

$$R_L = \frac{1}{1 + C_0 K_L} \tag{2}$$

$$q_e = K_F C_e^{\frac{1}{n}} \tag{3}$$

where q_e is the amount of target pollutant adsorbed on the adsorbent at equilibrium in mg/g; q_m is the maximum adsorption capacity in mg/g; K_L (L/mg) is the Langmuir adsorption constant related to the adsorption energy; C_e is the equilibrium concentration of the target pollutant in the solution phase in mg/L; R_L is the Langmuir equilibrium constant; C_0 is the initial concentration of the adsorbate in mg/L; K_F is the Freundlich equilibrium constant; $1/n$ is the coefficient relating to the adsorption strength (Li *et al.* 2015).

The fitting results for the Langmuir and Freundlich adsorption isotherm models are shown in Figure 10 and Table 3, respectively.

Table 2 | Comparison of the maximum adsorption capacities of different adsorbents

Adsorbents	Maximum adsorbate concentration (mg/L)	Maximum adsorption capacity q_{max} (mg/g)		References
		As(III)	As(V)	
Fe/Mn–CO$_3$-LDHs	50	120.13	47.03	This study
Mn–Fe-LDH	5	NA	2.26	Li (2010)
Zn–Fe-LDH		NA	1.01	
Mg–Fe-LDH		NA	0.89	
Mg/Al-LDO	50	NA	23.92	Sun *et al.* (2011)
NMMF	20	NA	0.55	Wang *et al.* (2016)
NMMB	40	NA	6.52	
Ti–Mn-LDH	10	38.76	NA	Li *et al.* (2012)
Mn–Fe-LDH	100	113.12	57.69	Otgonjargal *et al.* (2012)
Fe$_3$O$_4$/Cu(OH)$_2$	85, 45	37.97	42.90	Wang *et al.* (2015)
Fe@Cu oxide	75	55.04	50.58	Wu *et al.* (2019)
Fe@Cu&GO		70.36	62.60	
MgAl–MoS$_4$-LDH	400	99	56	Ma *et al.* (2017)

NA, data not available.
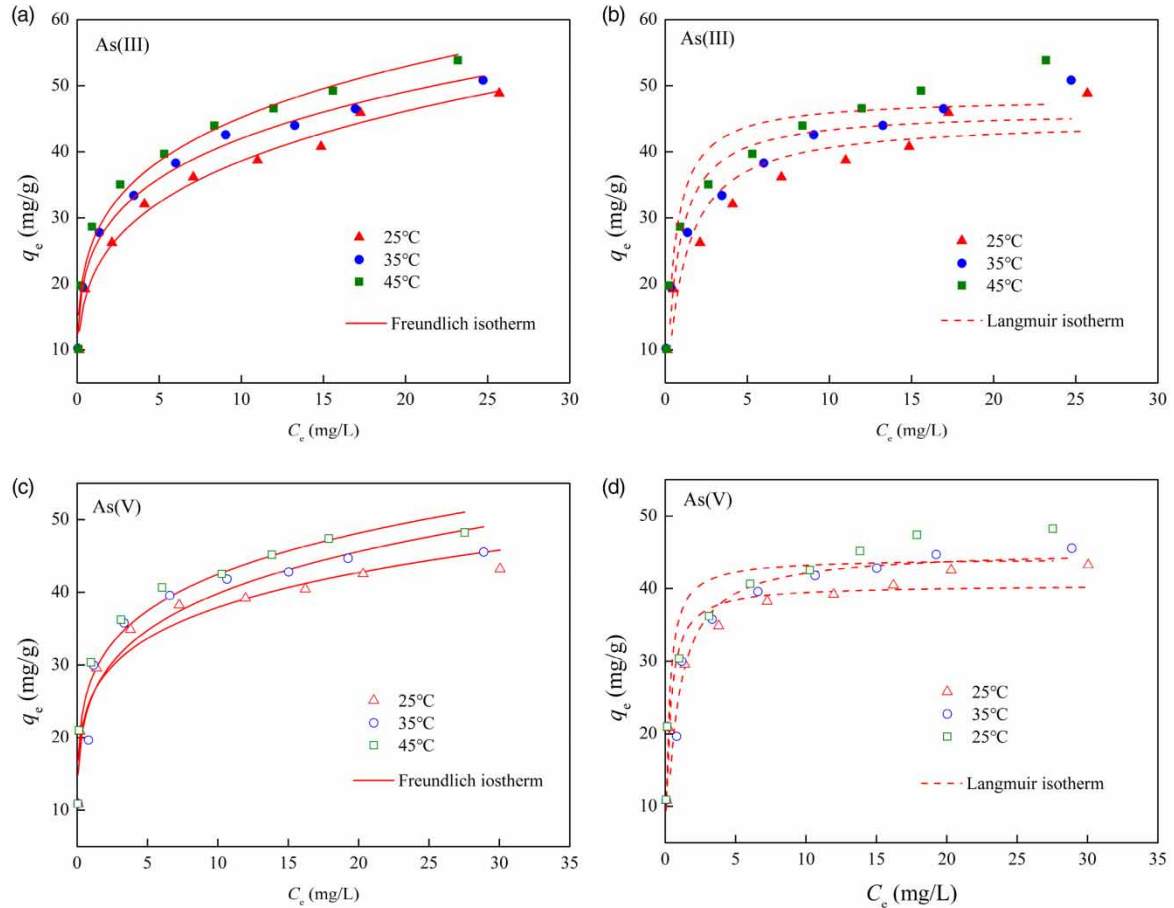
Figure 10 | Adsorption isotherm of As(III) and As(V) adsorption.

From Figure 10 and Table 3, it is clear that the As(III) adsorption isotherm on Fe/Mn–CO$_3$-LDHs conforms well to the Freundlich isothermal model (Figure 10 (a,c)), with the fitted correlation coefficient R^2 being always above 0.97, suggesting a nonuniform multilayer adsorption nature of As(III) on the material surface. The value of $1/n$ can be used to characterize the nonlinear growth trend of adsorption capacity (Crini 2008). The adsorption coefficients of As(III) remain between 0.1 and 0.5, indicating that the materials prepared in this laboratory readily adsorb As(III) under the studied conditions, with chemisorption being dominant. Under the same initial concentration, the increase in q_{max} with the increase of temperature further confirmed that the elevating temperature facilitated the adsorption of As(III) by the adsorbent and that the adsorption was an endothermic reaction.

As shown in Table 3, the correlation coefficients R^2 for both the Langmuir and Freundlich isotherm model fittings for As(V) adsorption were always >0.9, suggesting a significant correlation level. Nevertheless, the experimental data points strayed away from the fitted curves obtained by the Langmuir isotherm model at all

Table 3 | Fitting parameters for the Langmuir and Freundlich isotherm models

Fe/Mn–CO$_3$-LDHs	T (°C)	Langmuir			Freundlich		
		q_{max} (mg/g)	R_L (L/mg)	R_1^2	K_F (mg/g)	$1/n$	R_2^2
As(III)	25	44.9093	0.0206–0.1701	0.8776	21.3710	0.26	0.9827
	35	46.2559	0.0134–0.1172	0.8707	25.0461	0.22	0.9915
	45	48.1741	0.0099–0.0889	0.9018	26.7147	0.23	0.9733
As(V)	25	40.5110	0.0053–0.0475	0.9365	25.4923	0.17	0.9177
	35	45.3535	0.0147–0.1224	0.9247	25.3383	0.20	0.9125
	45	44.1720	0.0044–0. 0397	0.9030	27.9551	0.18	0.9492

temperatures, indicating that the As(V) adsorption by Fe/Mn–CO$_3$–LDHs could not be well described by the Langmuir model (Figure 10(b,d)).

The As(V) adsorption conformed better to the Freundlich isotherm model, manifesting the multimolecular layer adsorption nature. With the temperature rise, the adsorption capability of the adsorbent increased.

The thermodynamic parameters of adsorption are calculated from the linearized Van't Hoff equation (Equation (4)) and Gibbs free-energy equations (Equations (5) and (6)):

$$\ln K_d = \frac{-\Delta H}{RT} + \frac{\Delta S}{R} \tag{4}$$

$$\Delta G = -RT \ln K_d \tag{5}$$

$$K_d = K_F n \tag{6}$$

where ΔH, ΔS and ΔG represent the enthalpy (kJ/mol), entropy (J/mol/K) and free energy (kJ/mol) of adsorption, respectively; K_d is the equilibrium constant for adsorption; T is the temperature in K; R is the ideal gas constant.

In Table 4, the positive ΔH indicates that the adsorption of both As(III) and As(V) on Fe/Mn–CO$_3$-LDH is an endothermic reaction. ΔG has a value of around −12 kJ/mol, implying that the reaction is a spontaneous physisorption process. Furthermore, $\Delta S > 0$ indicates the incoherence of the reaction system. Therefore, the adsorption of As(III) and As(V) by Fe/Mn–CO$_3$-LDH is a predominantly physisorption process accompanied by chemisorption.

3.4. Adsorption kinetics

The pseudo-first-order (Equation (7)), pseudo-second-order (Equation (8)), Elovich (Equation (9)) and intra-particle diffusion (Equation (10)) kinetic models were employed to explore the adsorption reaction rates and reaction mechanism (Yu *et al.* 2011).

$$\ln (q_e - q_t) = \ln q_e - K_1 t \tag{7}$$

$$\frac{t}{q_t} = \frac{1}{q_e K_2} + \frac{1t}{q_e} \tag{8}$$

$$q_t = \frac{1}{\beta_E} \ln (\alpha_E \beta_E) + \frac{1}{\beta_E} \ln (t) \tag{9}$$

$$q_t = k_p t^{\frac{1}{2}} + C \tag{10}$$

where q_e is the equilibrium adsorption capacity in mg/g; q_t is the adsorption capacity at time t in mg/g; K_1 and K_2 are the rate constants; α_E is the initial adsorption rate in mg/(g·min); β_E is the surface coverage and activation energy-related constant in g/mg; k_p is the intra-particle diffusion rate constant in mg/(g·min$^{1/2}$); C is the boundary thickness–related constant in mg/g.

From the fitting results in Figure 11 and Table 5, it can be seen that the R^2 values of the adsorption data fitted by the pseudo-second-order kinetic equation at three initial concentrations (5, 10 and 50 mg/L) are all >0.998, suggesting that the model can well depict the removal behavior (Figure 11 (c,d)). The obtained theoretical equilibrium adsorption capacity q_e is almost approximate to the experimental value. K_2 is small, suggesting that the

Table 4 | Thermodynamic parameters of adsorption

	T (K)	ΔG (kJ/mol)	ΔH (kJ/mol)	ΔS (J/mol/K)
As(III)	298	−10.9239	13.747	83.151
	308	−12.1246		
	318	−12.5712		
As(V)	298	−12.4135	1.222	45.257
	308	−12.3983		
	318	−13.3393		
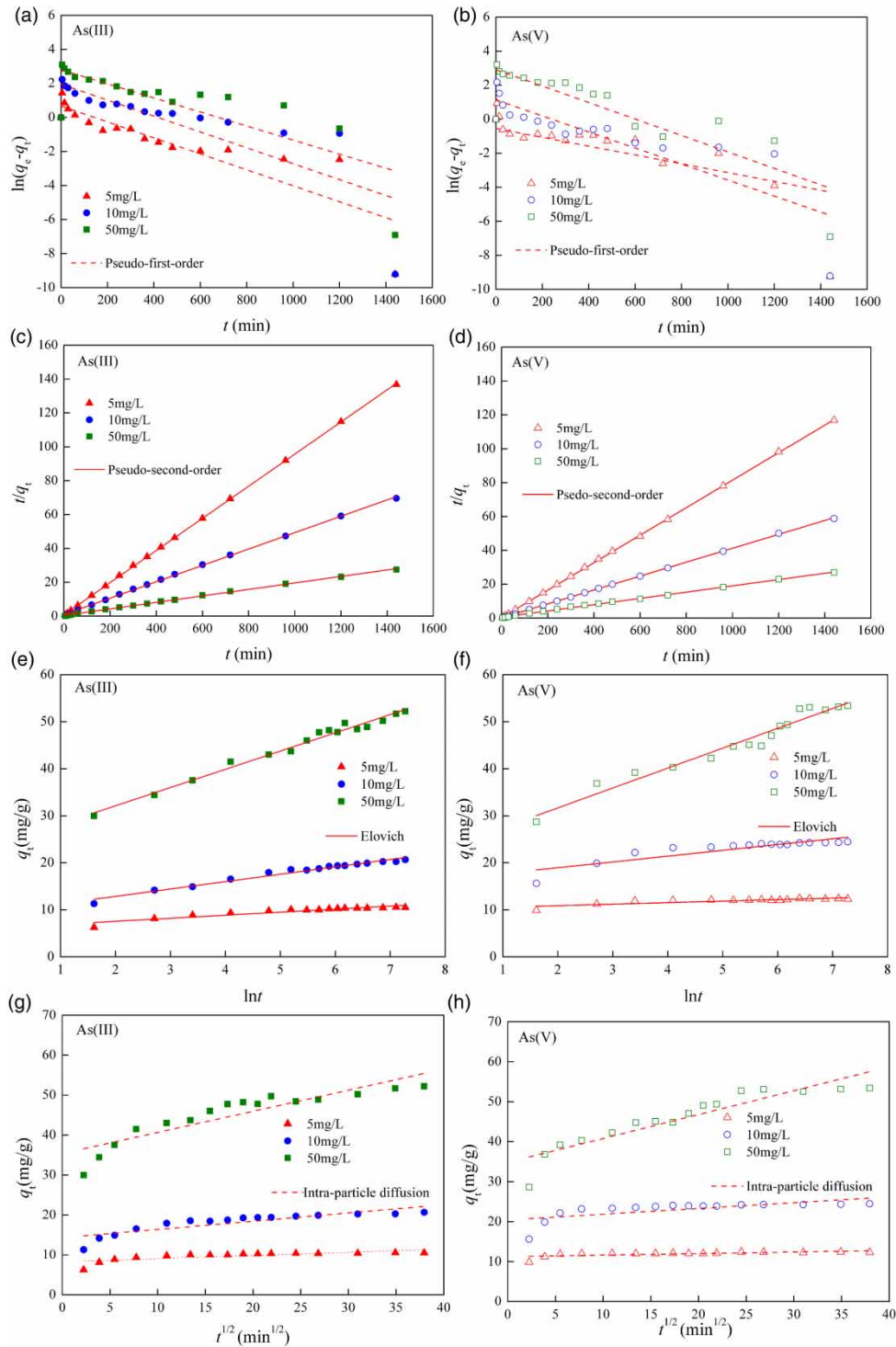
Figure 11 | Adsorption kinetics of As(III) and As(V) adsorption.

adsorption rate decreases with an increasing contact time and is proportional to the amount of adsorption sites. Therefore, the adsorption of As by Fe/Mn–CO₃-LDHs is a chemisorption-controlled process, with the adsorption capacity mainly determined by the surface active sites of the material (Hameed *et al.* 2007; Tan *et al.* 2008; Wang *et al.* 2020). As for the Elovich model (Figure 11 (e,f)), the value of the initial adsorption rate decreases significantly with the increase of the initial ion concentration and is extremely high at lower concentrations, indicating the presence of chemisorption. The fitted curve of pseudo-first-order kinetic equation (Figure 11 (a,

Table 5 | Fitting parameters for various adsorption kinetic models

Fe/Mn–CO₃-LDHs	C_0 (mg/L)	q_e (mg/g)	Pseudo-first-order model			Pseudo-second-order model		
			$q_{e,cal}$ (mg/g)	K_1 (min)	R^2	$q_{e,cal}$ (mg/g)	K_2 g/(mg·min)	R^2
As(III)	5	10.522	1.9686	0.0047	0.7517	10.5363	0.0109	0.9999
	10	20.672	7.0618	0.0047	0.6244	20.6697	0.0024	0.9994
	50	52.220	16.4974	0.0041	0.6024	52.1648	0.0008	0.9987
As(V)	5	12.320	0.5803	0.0026	0.2051	12.3122	0.0262	0.9999
	10	24.470	3.1146	0.0019	0.7000	24.3546	0.0087	0.9998
	50	53.440	18.5120	0.0048	0.7281	53.9374	0.0006	0.9982

Fe/Mn–CO₃-LDHs	C_0 (mg/L)	q_e (mg/g)	Elovich model			Intra-particle diffusion model		
			α_E mg/(g·min)	β_E (g/mg)	R^2	k_p mg/(g·min$^{1/2}$)	C (mg/g)	R^2
As(III)	5	10.522	10,058.3867	1.5396	0.8720	0.0795	8.2728	0.5590
	10	20.672	22,261.3109	1.0313	0.9697	0.2064	14.3203	0.7319
	50	52.220	2,083.4398	0.2578	0.9826	0.5283	35.3900	0.8001
As(V)	5	12.320	2.2468E + 13	3.1113	0.7077	0.0381	11.2615	0.4169
	10	24.470	790,338.5856	0.8106	0.7605	0.1433	20.4443	0.4294
	50	53.440	1,027.1147	0.2364	0.9559	0.5975	34.8438	0.8421

b)) and intra-particle diffusion are nonlinear (Figure 11 (g,h)), indicating that the adsorption process is influenced by the thickness of the boundary layer and involves multiple diffusive resistances.

4. CONCLUSION

By taking advantage of the intercalation capability of LDHs, the CO_3^{2-}- intercalated Fe–Mn bimetal LDH composite with the layered structure of hydrotalcite (Fe/Mn–CO₃-LDHs) was prepared using a co-precipitation method. The SEM results indicated that the single crystalline grain of the composite exhibited a plate-like morphology, with hexagonal crystalline characteristics and pores existing between lamellas. Minimal morphological changes were observed after As adsorption. At 25, 35 and 45 °C, when the initial concentrations of As(III) and As(V) ranged from 5 to 50 mg/L, the adsorption capacities of the Fe/Mn–CO₃-LDHs composite were 10.12–53.90 and 10.82–48.24 mg/g for As(III) and As(V), respectively. The adsorption process conformed well to the pseudo-second-order kinetic model and the Freundlich isotherm model. Based on a comprehensive analysis, the removal mechanisms include mainly electrostatic attraction, redox, surface complexation and ion exchange. At pH 7, As(III) was ligand-exchanged with hydroxyl groups on the surface of the metal laminate mainly in the form of H_3AsO_3, which then came into contact with Fe and was partially oxidized to As(V).

ACKNOWLEDGEMENTS

COMPETING INTEREST

The authors declare no competing interest.

DATA AVAILABILITY STATEMENT

All relevant data are included in the paper or its Supplementary Information.

REFERENCES

Anna, F. B., Marcello, G., Roberto, P. & Antonio, Z. 2006 Red mud and fly ash for remediation of mine sites contaminated with As, Cd, Cu, Pb and Zn. *Journal of Hazardous Materials* **B134**, 112–119.

Chandra, V., Park, J., Chun, Y. & Woo, J. 2010 Water-dispersible magnetite-reduced graphene oxide composites for arsenic removal. *ACS Nano* **4** (7), 3979.

Choong, T. S. Y., Chuah, T. G., Robiah, Y., Gregory, K. F. L. & Azni, I. 2007 Arsenic toxicity, health hazards and removal techniques from water: an overview. *Desalination* **217** (1–3), 139–166.

Crini, G. 2008 Kinetic and equilibrium studies on the removal of cationic dyes from aqueous solution by adsorption onto a cyclodextrin polymer. *Dyes and Pigments* **77** (2), 415–426.

Deng, H. M. 2019 Pollution status and detection technology of heavy metal elements in water environment. *World Nonferrous Metals* **2019** (13), 227–228.

Deng, L., Shi, Z., Wang, L. & Zhou, S. 2017 Fabrication of a novel $NiFe_2O_4$/Zn-Al layered double hydroxide intercalated with EDTA composite and its adsorption behavior for Cr(VI) from aqueous solution. *Journal of Physics and Chemistry of Solids* **104**, 79–90.

Dutta, P. K., Ray, A. K., Sharma, V. K. & Frank, J. M. 2004 Adsorption of arsenate and arsenite on titanium dioxide suspensions. *Journal of Colloid and Interface Science* **278** (2), 270–275.

Eleonora, D., Virginia, S. T. C. & Wolfgang, H. H. 2005 Removal of As(III) and As(V) from water using a natural Fe and Mn enriched sample. *Water Research* **39** (20), 5212–5220.

Goh, K. H., Lim, T. T. & Dong, Z. 2008 Application of layered double hydroxides for removal of oxyanions: a review. *Water Research* **42** (6–7), 1343–1368.

Halajnia, A., Oustan, S., Najafi, N., Khataee, A. R. & Lakzian, A. 2013 Adsorption–desorption characteristics of nitrate, phosphate and sulfate on Mg–Al layered double hydroxide. *Applied Clay Science* **80–81**, 305–312.

Hameed, B. H., Din, A. T. M. & Ahmad, A. L. 2007 Adsorption of methylene blue onto bamboo-based activated carbon: kinetics and equilibrium studies. *Journal of Hazardous Materials* **141** (3), 819–825.

Kameda, T., Saito, S. & Umetsu, Y. 2005 Mg-Al layered double hydroxide intercalated with ethylene-diaminetetraacetate anion: synthesis and application to the uptake of heavy metal ions from an aqueous solution. *Separation and Purification Technology* **47** (1–2), 20–26.

Li, X. J. 2010 *Study on the Adsorption Mechanism of Arsenic Removal from Aqueous Environment by Iron-Based LDH (in Chinese)*. Shaanxi Normal University, Xi'an.

Li, Y., Gao, B., Wu, T., Sun, D., Li, X., Wang, B. & Lu, F. 2009 Hexavalent chromium removal from aqueous solution by adsorption on aluminum magnesium mixed hydroxide. *Water Research* **43** (12), 3067–3075.

Li, X., Tang, Y. C., Huang, X. H., Wu, C. N. & Peng, Y. 2012 Removal of As (III) from water by using synthetically Ti-Fe hydroxide complexes. *Environmental Engineering* **30** (06), 60–64.

Li, F. Y., Xie, Y., Shi, L., Li, X. L., Li, F. R. & Wang, J. F. 2015 Adsorption of ammonia nitrogen in wastewater using rice husk derived biochar. *Chinese Journal of Environmental Engineering* **9** (3), 1221–1226.

Liu, J. M. 2015 *Study on Preparation, Characterization and Sulfate, Fluoride Adsorption by Layer Double Hydroxides*. Taiyuan University of Technology, Taiyuan.

Liu, G. F., Zhu, Z. Q., Zhao, N. N., Fang, Y. L., Gao, Y. Y., Zhu, Y. N. & Zhang, L. H. 2020 Mn-Fe layered double hydroxide intercalated with ethylene-diaminetetraacetate anion: synthesis and removal of As(III) from aqueous solution around pH 2–11. *International Journal of Aenvironmental Resarch and Public Health* **17** (24), 18.

Lv, L. 2005 *Adsorption and Ion-Exchange Behavior of Layered Double Hydroxides in the Uptake of Halide Anions from Aqueous Solution*. Beijing University of Chemical Technology, Beijing.

Ma, L., Islam, S. M., Liu, H., Zhao, J., Sun, G., Li, H., Ma, S. & Kanatzidis, M. G. 2017 Selective and efficient removal of toxic oxoanions of As(III), As(V), and Cr(VI) by layered double hydroxide intercalated with MoS_4^{2-}. *Chemistry of Materials* **29** (7), 3274–3284.

Maiti, A., Thakur, B. K., Basub, J. K. & De, S. 2013 Comparison of treated laterite as arsenic adsorbent from different locations and performance of best filter under field conditions. *Journal of Hazardous Materials* **262**, 1176–1186.

Nicomel, N. R., Leus, K., Folens, K., Van, D. V. P. & Du, L. G. 2015 Technologies for arsenic removal from water: current status and future perspectives. *International Journal of Environmental Research and Public Health* **13** (1), 62.

Ociński, D., Jacukowicz, S. I. & Kociołek, B. E. 2019 Freeze-drying as the post-processing technique improving adsorptive properties of waste Fe/Mn oxides entrapped in polymer beads towards As(III) and As(V). *Separation Science and Technology* **55** (3), 1–14.

Otgonjargal, E., Kim, Y. S., Park, S. M., Baek, K. & Yang, J. S. 2012 Mn–Fe layered double hydroxides for adsorption of As(III) and As(V). *Separation Science and Technology* **47** (14–15), 2192–2198.

Patel, R., Inamdar, A. I., Hou, B., Cha, S., Ansari, A. T., Gunjakar, J. L., Im, H. & Kim, H. 2017 Solvothermal synthesis of high-performance Ni-Co layered double hydroxide nanofoam electrode for electrochemical energy storage. *Current Applied Physics* **17** (4), 501–506.

Qi, P. & Pichler, T. 2016 Competitive adsorption of As(III) and As(V) by ferrihydrite: equilibrium, kinetics, and surface complexation. *Water, Air, & Soil Pollution* **227** (10), 387.

Sankpal, U. T., Pius, H., Khan, M., Shukoor, M. I., Maliakal, P., Lee, C. M., Abdelrahim, M., Connelly, S. F. & Basha, R. 2012 Environmental factors in causing human cancers: emphasis on tumorigenesis. *Tumour Biology* **33** (5), 1265–1274.

Singh, R., Singh, S., Parihar, P., Singh, V. P. & Prasad, S. M. 2015 Arsenic contamination, consequences and remediation techniques: a review. *Ecotoxicology and Environmental Safety* **112**, 247–270.

Smedley, P. L. & Kinniburgh, D. G. 2002 A review of the source, behaviour and distribution of arsenic in natural waters. *Applied Geochemistry* **17** (5), 517–568.

Sun, Y. Y., Zeng, X. B. & Bai, L. Y. 2011 Adsorption of arsenate from aqueous solution by Mg/Al layered double oxide. *Acta Scientiae Circumstantiae* **31** (07), 1377–1385.

Tan, I. A. W., Ahmad, A. L. & Hameed, B. H. 2008 Adsorption of basic dye on high-surface-area activated carbon prepared from coconut husk: equilibrium, kinetic and thermodynamic studies. *Journal of Hazardous Materials* **154** (1–3), 337–346.

Tang, J., Zhang, L., Zhang, J., Ren, L., Zhou, Y., Zheng, Y., Luo, L., Yang, Y., Huang, H. & Chen, A. 2020 Physicochemical features, metal availability and enzyme activity in heavy metal-polluted soil remediated by biochar and compost. *Science of The Total Environment* **701**, 134751.

Wan, S., Wang, S., Li, Y. & Gao, B. 2017 Functionalizing biochar with Mg–Al and Mg–Fe layered double hydroxides for removal of phosphate from aqueous solutions. *Journal of Industrial and Engineering Chemistry* **47**, 246–253.

Wang, T., Yang, W., Song, T., Li, C., Zhang, L., Wang, H. & Chai, L. 2015 Cu doped Fe_3O_4 magnetic adsorbent for arsenic: synthesis, property, and sorption application. *RSC Advances* **5** (62), 50011–50018.

Wang, S., Gao, B. & Li, Y. 2016 Enhanced arsenic removal by biochar modified with nickel (Ni) and manganese (Mn) oxyhydroxides. *Journal of Industrial and Engineering Chemistry* **37**, 361–365.

Wang, X. H., Yang, X., Wang, C. & Tian, Y. 2020 Effects and mechanisms of methyl orange removal from aqueous solutions with modified coconut shell biochar. *Science Technology and Engineering* **20** (27), 11371–11377.

Wen, Z., Zhang, Y., Dai, C., Chen, B., Guo, S., Yu, H. & Wu, D. 2014 Synthesis of ordered mesoporous iron manganese bimetal oxides for arsenic removal from aqueous solutions. *Microporous and Mesoporous Materials* **200**, 235–244.

Wu, K., Jing, C., Zhang, J., Liu, T., Yang, S. & Wang, W. 2019 Magnetic Fe_3O_4@CuO nanocomposite assembled on graphene oxide sheets for the enhanced removal of arsenic(III/V) from water. *Applied Surface Science* **466**, 746–756.

Xu, Z., Li, Q., Gao, S. & Shang, J. K. 2010 As(III) removal by hydrous titanium dioxide prepared from one-step hydrolysis of aqueous TiCl(4) solution. *Water Research* **44** (19), 5713–5721.

Yu, X. Y., Luo, T., Jia, Y., Zhang, Y. X., Liu, J. H. & Huang, X. J. 2011 Porous hierarchically micro-/nanostructured MgO: morphology control and their excellent performance in As(III) and As(V) removal. *The Journal of Physical Chemistry* **115** (45), 22242–22250.

Zeng, H., Xu, K., Wang, F. H., Sun, S. Q., Li, D. & Zhang, J. 2021 Preparation of adsorbent based on water treatment residuals and chitosan by homogeneous method with freeze-drying and its As(V) removal performance. *International Journal of Biological Macromolecules* **184**, 313–324.

Zhang, G. C. 2012 *Study on Preparation and Sorption Behavior of Sodium Dodecylsulfonate Intercalated Organo Layered Double Hydroxide*. Shangdong University, Jinan.

Zhang, J. 2018 *The Performance and Mechanism for the Removal of As (III)/As (V) From Water by GO&FeCu*. Xi'an University of Architecture and Technology, Xi'an.

Zhang, W., Singh, P., Paling, E. & Delides, S. 2004 Arsenic removal from contaminated water by natural iron ores. *Minerals Engineering* **17** (4), 517–524.

Zhu, J., Lou, Z. M., Wang, Z. H. & Xu, X. H. 2014 Preparation of iron and manganese oxides/carbon composite materials for arsenic removal from aqueous solution. *Progress in Chemistry* **26** (09), 1551–1561.